CrossMark

Click for updates

International Journal of Image and Data Fusion

Building damage assessment after the earthquake in Haiti using two post-event satellite stereo imagery and DSMs

Jiaojiao Tian[a], Allan A. Nielsen[b] & Peter Reinartz[a]

[a] Remote Sensing Technology Institute, German Aerospace Center (DLR), Wessling, Germany

[b] Department of Applied Mathematics and Computer Science, Technical University of Denmark, Lyngby, Denmark
Published online: 30 Mar 2015.

PLEASE SCROLL DOWN FOR ARTICLE

Taylor & Francis
Taylor & Francis Group

RESEARCH ARTICLE

Building damage assessment after the earthquake in Haiti using two post-event satellite stereo imagery and DSMs

Jiaojiao Tian[a]*, Allan A. Nielsen[b] and Peter Reinartz[a]

[a]*Remote Sensing Technology Institute, German Aerospace Center (DLR), Wessling, Germany;*
[b]*Department of Applied Mathematics and Computer Science, Technical University of Denmark, Lyngby, Denmark*

In this article, a novel after-disaster building damage monitoring method is presented. This method combines the multispectral imagery and digital surface models (DSMs) from stereo matching of two dates to obtain three kinds of changes: collapsed buildings, newly built buildings and temporary shelters. The proposed method contains three basic steps. The first step is to focus on the DSMs and orthorectified images preparation. The second step is to segment the panchromatic images in obtaining small homogeneous regions. In the last step, a rule-based classification is built on the change information from iteratively reweighted multivariate alteration detection (IR-MAD) and height to extract the three kinds of changes. To further improve the accuracy of the results, a region-based grey-level co-occurrence matrix texture measurement is used. The proposed method is applied to monitor building changes after the 2010 Haiti earthquake, and the obtained results are further evaluated both visually and numerically.

Keywords: building damage; change detection; digital surface models; segmentation

1. Introduction

Building damage assessment is very important after natural or man-made disaster events, like earthquakes and conflicts. There is a demand for updating existing databases and providing rapid mapping of urban changes after disasters. Remote sensing techniques are providing many possibilities for change monitoring (Singh 1989, Coppin *et al.* 2004). A popular technique to obtain the changes after a disaster is to compare the pre-event very high-resolution (VHR) imagery with the post-event VHR imagery and has been explored since a long time (Gamba and Casciati 1998, Turker and San 2003). In recent years, many more studies have been performed in order to generate change maps using different kinds of data and methods (Brunner *et al.* 2010, Dell'Acqua *et al.* 2010, Rastiveis *et al.* 2013). However, collapsed or damaged buildings can be hardly distinguished from intact ones in high-dense building areas. This is due to the fact that changed buildings still share similar radiometric information with unchanged buildings and roads. Moreover, after earthquakes, building changes are mixed with many other changes, including changes influenced by the earthquake, like road damages, and changes not influenced by the earthquake, like seasonal changes.

In order to overcome these problems, height information from digital surface model (DSM) has been employed in disaster monitoring in many applications. Knudsen and Olsen (2003) used the DSM from LiDAR data in extracting the building boundaries, which can be compared with existing pre-event building footprint data to generate a

---

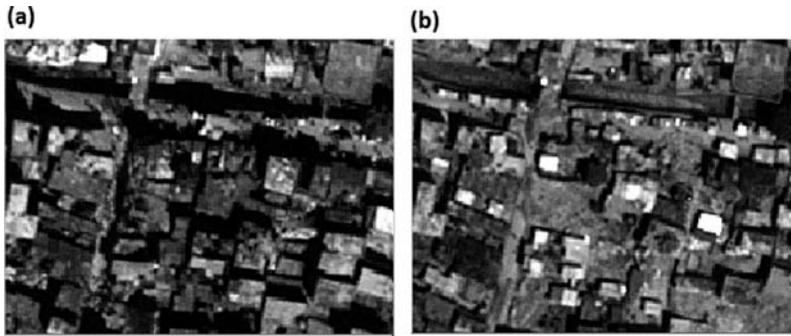*Corresponding author. Email: Jiaojiao.Tian@dlr.de

Figure 1.   Example of the changes in high-dense building area (left: 6 days after earthquake, right: half year after earthquake).

change map. Another possibility is to directly use two DSMs from LiDAR to calculate the height changes (Murakami *et al.* 1999). But due to the high cost of LiDAR data, and low availability of building footprint data, these methods can be hardly applied in not highly developed areas for disaster assessment. Turker and Cetinkaya (2005) and Tong *et al.* (2012) tried to use the DSM from stereo imagery, but the test area they used was much simpler with large buildings in regions with low building density. For a damaged building area like in Port-au-Prince, Haiti, where very dense and complex building heights are present (as shown in Figure 1), these methods are not adequate. In ideal cases with very good DSM representations, a direct DSM subtraction could already generate a reliable change map. But the accuracy of the detection results is highly dependent on the DSM quality, which often contain insufficient height information if generated from spaceborne imagery (d'Angelo *et al.* 2008).

In many cases, no proper pre-event high-resolution satellite/airborne images, DSMs or vector (geographic information system) data of buildings are available for comparing and evaluating the damages. Hussain *et al.* (2011) extracted buildings in Port-au-Prince area by using GeoEye-1 imagery and LiDAR data. However, due to the lack of pre-event data, no change detection has been performed.

Several automatic change detection techniques using DSM data additionally to multispectral information have been developed in our previous work and can be used in this context (Chaabouni-Chouayakha *et al.* 2013, Tian *et al.* 2011, 2014a, 2014b, Tian 2013). But these methods have to be further developed in order to cope with the challenges shown in Figure 1. Therefore, in this article, we present a new approach for monitoring collapsed buildings and newly built constructions with examples from the earthquake in Haiti by using two pairs of post-event stereo imagery. One was acquired directly after the earthquake and the other was acquired half a year later. After half a year, many of the collapsed buildings were removed or rebuilt, and some quickly built buildings and temporary shelters/tents are constructed. These temporary living places are always located in parks or on squares after cutting down some trees or cleaning several small collapsed buildings. Therefore, the appearance of these temporary shelters may not lead to large height change, but to spectral and texture change. The monitoring of the removed buildings can provide better destroyed building assessment, and the monitoring of newly built buildings and temporary shelters can also help government management and city planning.

As mentioned before, the DSMs generated from stereo data show lower quality than DSMs from LiDAR data, especially in high-dense building areas. The aim of this article was therefore also to generate a robust damage assessment map by fusing the height change information from spaceborne DSMs with lower quality together with texture information from orthorectified satellite images.

For this purpose, we adopt a region-based change detection method (Tian 2013) and further improve the workflow for disaster monitoring. To eliminate the influence from vegetation and shadows, these regions are extracted with multispectral information and labelled before performing a mean shift segmentation. In the region-based change detection procedure, we use iteratively reweighted multivariate alteration detection (IR-MAD) to combine the change vectors from images and DSM, and finally the units are classified into collapsed buildings, newly built buildings and temporary shelters. These temporary shelters are relatively difficult to detect correctly due to their small size and low height. In order to refine this class changes, we use a region-based texture measurement to further refine the result. After presenting the used data-sets, the methodology is described in detail followed by the experiments, result evaluation, validation and finally discussion.

2. Data-sets

A very strong earthquake in Haiti (Corbane *et al.* 2011, Voigt *et al.* 2011) struck the city of Port-au-Prince on 12 January 2010 and induced heavy damages to buildings. For the investigation, a dense city area within Port-au-Prince is chosen. Two dates of GeoEye-1 stereo images with 0.5-m resolution are used. One was obtained 6 days after the earthquake, and the area chosen contains many collapsed buildings. The second data were acquired on 18 August 2010, when several collapsed buildings are in the process of reconstruction. In addition, in the later data-set, many regions with high-density shelters can be found, which were built as temporary habitations for the local residents.

A reference airborne LiDAR point cloud data have been obtained from OpenTopography website. These data were originally provided by the Rochester Institute of Technology (RIT) and Kucera International under subcontract to ImageCat, Inc. (OpenTopography 2011).

The investigated changes in this test region are composed of three classes. The first class comprises the collapsed buildings during the earthquake. After half year, the remains have been cleared away. The second class consists of newly built buildings. Some reconstruction work is supposed to have been carried out after the earthquake. The last class is temporary shelters. Since many buildings are destroyed, it is difficult to rebuild enough buildings for the local residents in a short period. Thus, many temporary shelters can be found in the images from Date 2.

Change detection in this test region is quite challenging. As shown in Figure 2, in this densely structured city urban region, many buildings do not exhibit clearly visible roof edges and are often connected with their neighbouring buildings. Moreover, buildings in the test region are mainly of small size and show low height values. All these mentioned characteristics challenge the efficiency and accuracy of automatic (but also manual) building change detection methods.
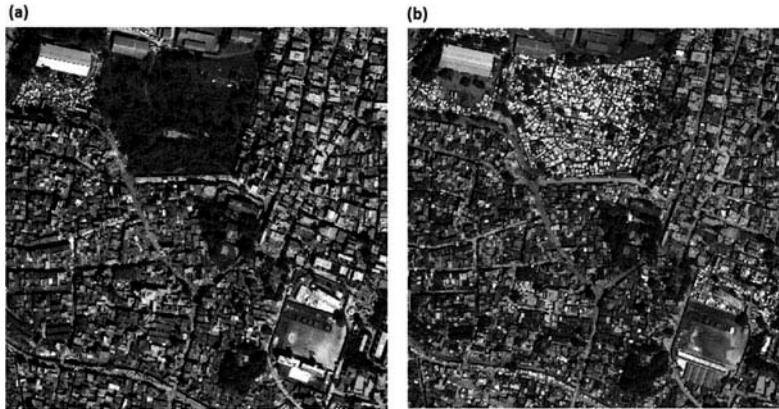
Figure 2.   Panchromatic images of the test area: (a) 6 days after the earthquake; (b) half year after the earthquake (1000 × 1000 pixels).

3.   Methodology

There are three main steps in our approach. The first step is image preprocessing, in which the DSM generation and image preparation are described. Second, in order to perform the region-based change detection, the original regions are generated based on mean shift segmentation from orthorectified panchromatic images. Finally, changes are classified as collapsed buildings, newly built buildings and temporary shelters by fusing change information from DSM and orthorectified original images.

3.1.   Pre-processing

Height information from DSM is essential for building monitoring. In the preprocessing step, the DSMs here are generated from satellite stereo imagery by the semi-global matching (SGM) method (Hirschmüller 2008), which shows robustness and high matching density. It has been implemented in several versions, among which we use the one developed by d'Angelo *et al.* (2008, 2011). The DSMs generated from January and August are further coregistered to remove any shift in three dimensions (Tian 2013). In this coregistration procedure, LiDAR data that have been mentioned in the last section are used as reference. DSMs from Date 1 and Date 2 are coregistered to the LiDAR-DSM. These two prepared DSMs are displayed in Figure 3a and b, respectively.

As can be seen from Figure 3, roads and buildings can be roughly separated according to their height information. However, we cannot get a clear boundary due to the high building density. Thus, direct height subtraction will not be sufficient in detecting building changes, due to low sharpness in building representation. Thus, in the following step, more information from the satellite images is extracted and adopted for change detection. To guarantee that all corresponding pixels represent the same geographical location, the panchromatic and multispectral images are orthorectified based on the generated DSMs and shifted correspondingly using the shift values from DSM coregistration.
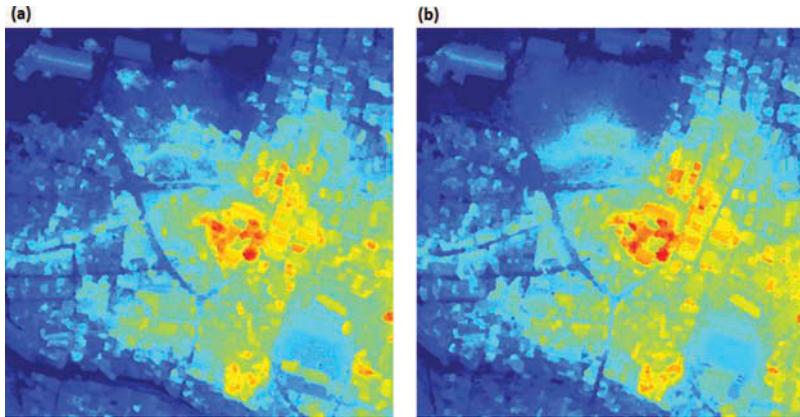
Figure 3. Generated DSMs of the test area: (a) 6 days after the earthquake; (b) half year after the earthquake.

3.2. Segmentation

As illustrated above, the generated DSMs are indicating elevation values in the building region, but one of the main disadvantages of these spaceborne DSMs is the blurred boundaries of buildings. To overcome this problem, the original satellite images can be introduced to the change detection workflow. Poli and Soille (2012) have proven that segmentation results from VHR images can be used to improve the DSM quality generated from stereo imagery. In this article, the segmentation aims to produce small units that have different spectral or textural characters from the areas nearby. Based on these units (segments), change features and change probabilities can be further analysed. The segmentation is carried out based on the orthorectified panchromatic images that are prepared as described in the last section. The mean shift algorithm from EDISON library (Comaniciu and Meer 2002) is adopted to obtain potentially small change units due to its good performance. Figure 4 shows an example of how segmentation improves the DSM quality. Figure 4a and b is the orthorectified panchromatic image and the initially generated DSM. Figure 4d is the reference DSM from LiDAR (LiDAR-DSM). After segmentation, we calculate the average elevation values for each segment. The refined DSM is shown in Figure 4c. As can be seen, the building boundaries are much sharper than before and buildings are better represented. To study the improvement in detail, the profile comparisons of two buildings are shown in Figure 5. These two buildings have been marked in Figure 4a with yellow lines. In Figure 5, the elevation values of the original DSM, refined DSM and reference LiDAR-DSM are plotted with colours red, blue and green, respectively. Figure 5a depicts that although the original DSM matches better with the LiDAR-DSM in height along the selected profile, the refined DSM presents the building boundaries better. Since we take average values for each segment, the obtained height can be little higher or lower than the reference DSM. But this kind of small height difference will not significantly influence the final change detection results. The improvement in the refined DSM distinguishes better for a certain building, as is shown in the right part of Figure 5b, the refined DSM and the LiDAR-DSM match well in the stepwise height distribution.
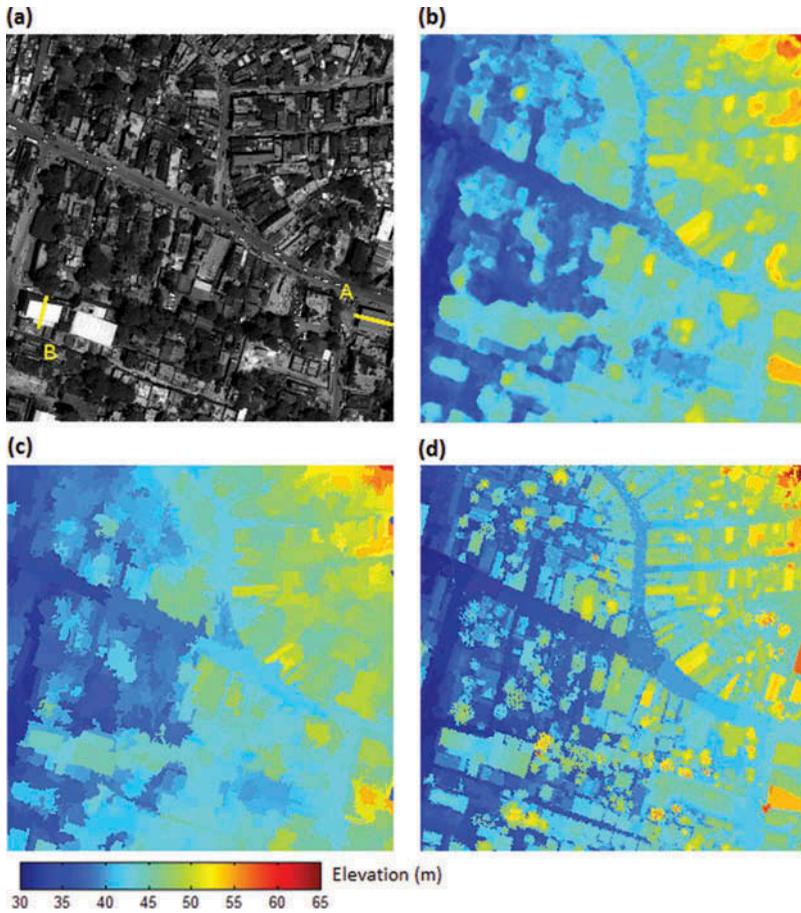
Figure 4. DSM quality improvement: (a) panchromatic image; (b) original generated DSM; (c) refined DSM; and (d) reference DSM from LiDAR.
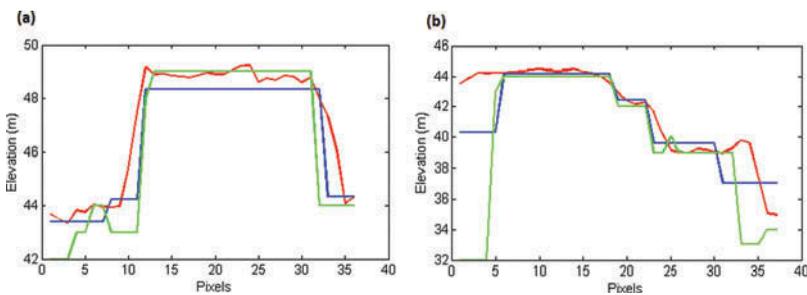

Figure 5. Profile comparisons of building A (a) and building B (b) along the yellow lines in Figure 4a (red: original DSM; blue: refined DSM; green: reference LiDAR-DSM).

As only building changes are of interest in this work, small segments in the vegetation or shadow regions bring unnecessary computational burden and may also introduce errors to the building change detection results. In the segmentation procedure, we therefore additionally use the land-cover classes: shadow and vegetation derived from multispectral images. These shadow and vegetation regions are first labelled (shown in black colour in Figure 6b) as separated segments and will not be further segmented and analysed.

The change detection workflow is described in Figure 7. Since the boundary of the collapsed buildings is better displayed in Date 1 image and the boundary of newly built
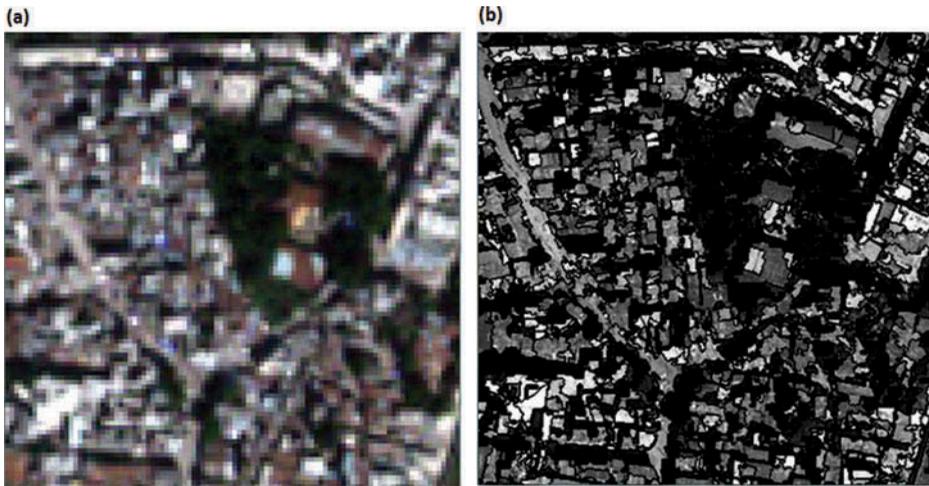

Figure 6. Segmentation results (b) of a subtest region (a).
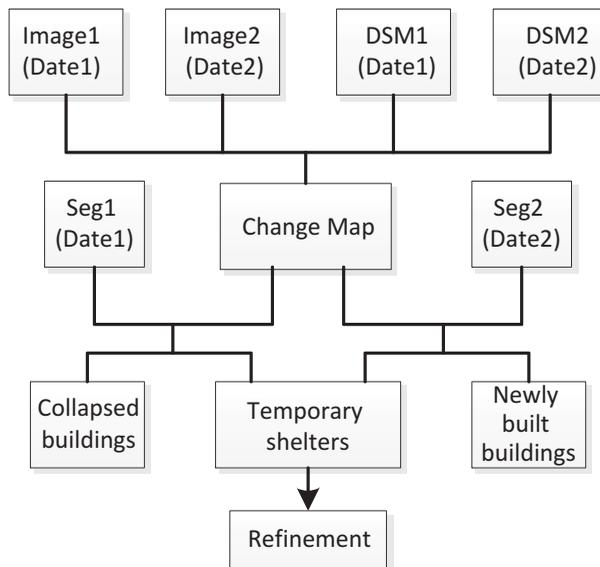

Figure 7. Building change detection and classification workflow.

buildings or shelters is shown only in Date 2 imagery, the segmentation procedure has been applied to both data, respectively. The extracted changes are further analysed and combined to generate the final change result.

3.3. Change classification

IR-MAD has been introduced by Nielsen (2007) to highlight changes, which has been proven to be an effective linear change detection method. This method mainly aims at establishing a reliable background estimation method of no change, thus to identify the real changes and reduce false alarms.

As the most important advantage, IR-MAD is an unsupervised change detection method. It considers all of the feature channels generated from the images (DSM, texture, spectral channels, etc.) of the two dates $F = (F_1, F_2, F_3, ... F_k)^{\mathrm{T}}$ and $G = (G_1, G_2, G_3, ... G_k)^{\mathrm{T}}$. The changes can be expressed by the linear combination of F and G (shown in Equation (1)). a_i and b_i are the coefficients calculated by applying canonical correlation analysis.

$$\begin{bmatrix} F \\ G \end{bmatrix} \Rightarrow \begin{bmatrix} a_1^{\mathrm{T}}F - b_1^{\mathrm{T}}G \\ . \\ . \\ . \\ a_k^{\mathrm{T}}F - b_1^{\mathrm{T}}G \end{bmatrix} \tag{1}$$

IR-MAD is an iterative scheme to put large weights on areas that show little change over time. This weight will be included in the calculation of mean, variance and covariance. The iteration will stop when the largest absolute change in the canonical correlation reaches a preset value, e.g. 10^{-6}. We use the chi-square distance for all of the MAD components as the extracted change map.

As shown in Figure 7, besides the multispectral bands of the satellite image, the change information from panchromatic images and the DSMs is also adopted as change features. As indicated in the workflow in Figure 7, the generated change map is combined with the segmentation result from two dates, respectively, to classify the changes. The changed regions with height decrease are classified as collapsed buildings, the regions that exhibit height increase are classified as the newly built ones, these regions show high values in the change map, while the regions that exhibit no changes in height are classified as temporary shelters. Since many regions belong to the temporary shelters, a texture-based refinement is performed to improve the overall accuracy.

Grey-level cooccurrence matrix (GLCM) is one of the popular and robust texture features. It estimates the second-order statistics properties by calculating the frequency of pixels in different levels cooccurrence in a designed distance within a given window (Haralick *et al.* 1973). In many cases, the window size will directly influence the efficiency of the usage of texture features. In this article, instead of selecting the window size, we calculate the region-based GLCM features (Bignami *et al.* 2011). All of the pixels inside one region are used in the cooccurrence matrix generation. After we get the cooccurrence matrix, the second-order statistics can be derived from it. Here, we use the 'homogeneity' feature, since it has proven to show a good performance in building change detection (Matikainen *et al.* 2010).

$$\text{Homogeneity: } \sum_{i,j=0}^{N-1} \frac{P_{i,j}}{1+(i-j)^2} \qquad (2)$$

$$\text{in which } P_{i,j} = \frac{V_{i,j}}{\sum_{i,j=0}^{N-1} V_{i,j}};$$

i is the row number;

j is the column number;

$V_{i,j}$ is the number of the occurrence in the GLCM matrix at the position (i, j);

$P_{i,j}$ stands for the normalised value of $V_{i,j}$.

4. Experiments

4.1. Results

The proposed method is applied on the Haiti test region. In the change classification procedure, we take the changed regions with more than 2-m height increase as newly built buildings. The collapsed buildings are the changed regions with more than 2-m height decrease. The remaining changed regions are temporary shelters, which have been further improved by using the GLCM texture. Figure 8 shows the change detection results. Figure 8a and c shows the detected collapsed buildings and newly built buildings, respectively. Figure 8b and d shows the temporary shelters detected by using the segmentation results from Date 1 and Date 2, respectively. Many detected changes shown in Figure 8b and d are similar, but the building shapes are different due to the changes during this half year. By comparing these two masks, the detected temporary shelters can be classified to three types: (1) detected in both masks, (2) only shown in the mask of Figure 8b and (3) only shown in the mask of Figure 8d. As a further refinement, GLCM homogeneity features are calculated, respectively, based on the regions from these three classes.

The final change detection result including the collapsed buildings (marked in red), newly built buildings (marked in blue) and temporary shelters (marked in green) is shown in Figure 9. This result has been projected to Date 2 panchromatic image. The detected change areas match well with a visual interpretation of the image.

4.2. Results evaluation

For further evaluation, reference maps have been manually extracted in three small test regions, as it is difficult to obtain change reference data for the whole test region. Additionally, in some places, it is even visually difficult to identify building changes based solely on satellite images. Therefore, three subregions are selected for evaluating the obtained change detection results numerically, as shown in Figure 10. Unfortunately, without precise height change reference data, it is very difficult to evaluate the obtained results, especially for separating the newly built buildings and newly built temporary shelters. These two classes mainly differ in height, which can be hardly observed from optical images, as our change reference data are obtained by manually comparing two orthorectified images. Therefore, in the results evaluation
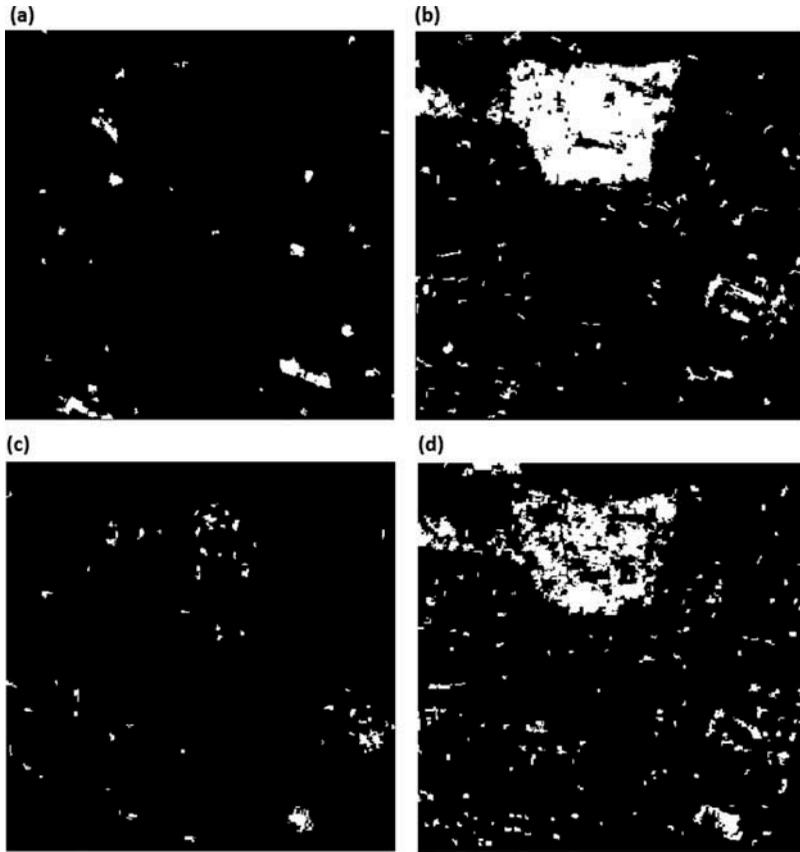
Figure 8.　Original change masks: (a) collapsed building mask; (b) temporary buildings based on Seg1; (c) newly built building mask; (d) temporary buildings based on Seg2.

procedure, in order to get some meaningful numerical evaluation result, we have combined these two classes as 'newly built'.

Figure 10 shows the panchromatic images in the first and second columns, and the third and fourth columns display the detection results of collapsed buildings and newly built constructions, respectively. The detected results are displayed together with the change reference data. In the figures of third and fourth columns, the green colour represents true detected, blue colour pixels are the false negatives, and red colour pixels are the false alarms. Table 1 shows quantitative evaluation results for these three regions. Since the number of collapsed buildings is small, it is very difficult to rate the results. For 'newly built', a true detection rate between 78% and 93% can be reached, but the false alarm rate is still a little high. Since it is a fully automatic method, it could still be used in addition to visual interpretation in case of rapid mapping of damages after large earthquake events to get hints where the mainly effected regions and even single destroyed houses are located.

To further evaluate the proposed method, we compare it with the method described in Tian *et al.* (2013). In that paper, the change detection map is generated
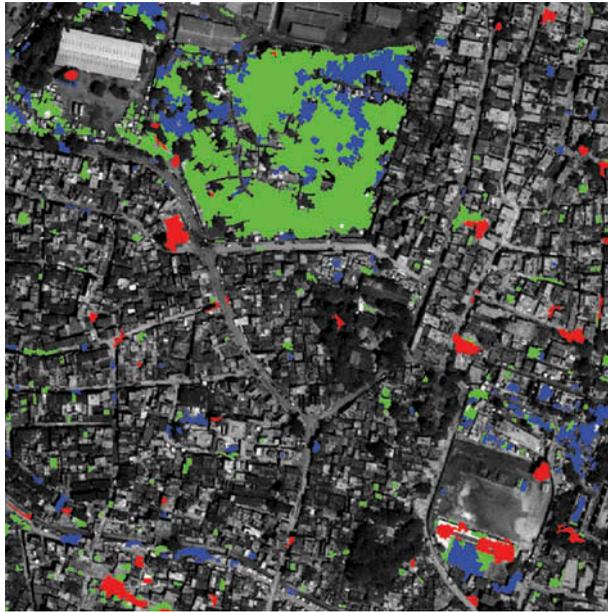
Figure 9. Change detection results: red: collapsed buildings; blue: newly built buildings; green: temporary shelters.
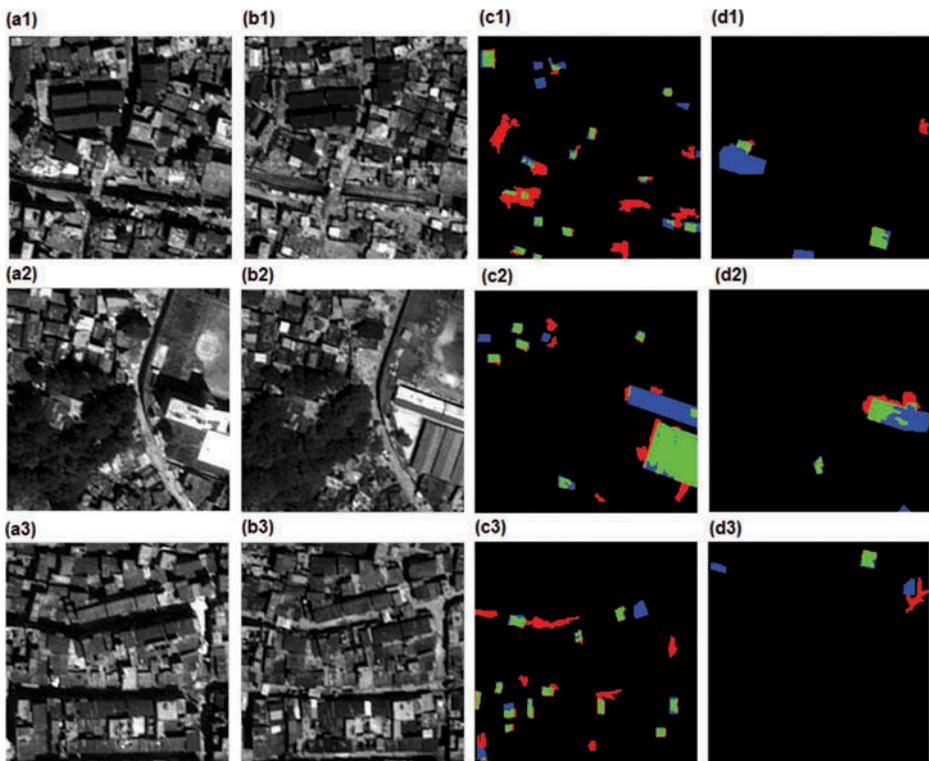
Figure 10. Change detection result evaluation in three subregions (green: true detected; red: false alarm; blue: false negative).

J. Tian et al.

Table 1. Detection rates of collapsed and newly - built constructions.

| Test regions | Classes | True detected (object) | | False detected (object) | |
		Number	Rate [%]	Number	Rate [%]
1	Collapsed	2	66.67	1	33.33
	Newly built	15	78.95	4	21.05
2	Collapsed	2	66.67	0	0
	Newly built	7	77.78	4	33.33
3	Collapsed	1	33.33	1	50.00
	Newly built	13	92.86	5	27.78

by using the weighted change vector analysis based on height change and texture change features. The regions map is prepared by merging segmentation results of two panchromatic images. The final region-based change detection probability map has values from 0 to 1. By manually giving a threshold T on the probability map, a final change detection mask can be generated. Only positive changes are of interest in that paper. Therefore, as a comparison, based on the method used in Tian *et al.* (2013), we generate the positive change (newly built) probability map for the three test regions of Figure 10.

For a fair comparison, a series of change detection masks is generated by using different threshold values. The numbers of true detected and false detected objects are counted to evaluate the accuracy of these masks. These numbers are described in Figure 11, in which the dark grey lines connect values of the true detected object numbers, while the false detected object numbers are connected with light grey lines. These numbers can be compared with the results described in Table 1. As described, in the test region 1, the proposed method is able to correctly detect 15 newly built objects with only 4 false alarms. In Figure 11, when $T = 0.25$ is chosen, we get the same number of true detected newly built objects, but 13 false alarms. Similar results are achieved for test region 3, the proposed method results in 13 true detected newly built objects and 5 false detections. In Figure 11, the best combination is 13 true detections and 7 false detections. In test region 2, the advantage of the proposed method is not as obvious as in the other two regions.
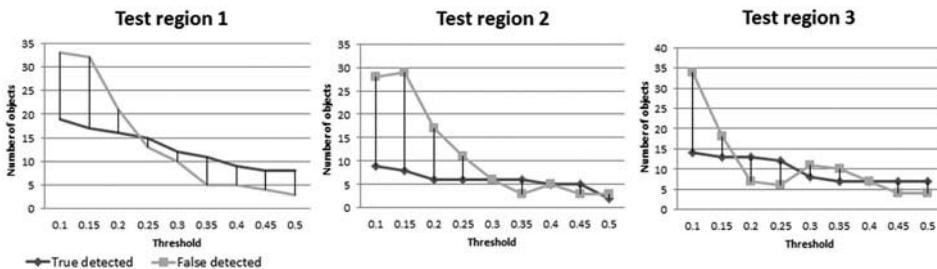
Figure 11. Performance of exiting method (Tian *et al.* 2013) for the Haiti data.

5. Discussion and conclusion

The region-based change detection method developed in this article shows promising results when applied to monitor changes between two post-event satellite stereo imagery of the 2010 Haiti earthquake. It has to be mentioned that both segmentation and DSM generation are very challenging in the Haiti region due to the high density and small size of the buildings, thus influencing the 3D change detection results. The proposed method has proven its robustness also in case of locally small changes. Three kinds of changes can be detected: collapsed buildings, newly built buildings and temporary shelters. All of these changes are essential for crisis management and scientific research.

The DSM from stereo matching can provide important height information by efficiently separating the collapsed buildings, newly built buildings and temporary shelters. Panchromatic image-based segmentation can classify the area in homogeneous regions. Using the average height from these regions can cover some quality drawbacks of the DSMs. Integration of the region-based GLCM texture in change refinement has also shown to be able to refine the change detection results especially for temporary shelters.

Monitoring building changes efficiently and accurately is very important for disaster monitoring. Moreover, the distinguishing of various building change types enriches information assessment for disaster monitoring and city planning. The initial results are extracted and presented in this article. However, due to the lack of reference data, the evaluation has been performed for only two classes. Further evaluation should be processed when LiDAR data from both pre- and post-change are available. In addition, the developed methodology will in future be applied to compare the pre-event images and post-event images. It may give a rapid assessment of building changes in similar situations if stereo images are available.

Acknowledgements

References

Bignami, C., *et al.*, 2011. Objects textural features sensitivity for earthquake damage mapping. *In*: *Joint urban remote sensing event (JURSE)*, 11–13 April, Munich, 333–336.

Brunner, D., Lemoine, G., and Bruzzone, L., 2010. Earthquake damage assessment of buildings using VHR optical and SAR imagery. *IEEE Transactions on Geoscience and Remote Sensing*, 48 (5), 2403–2420. doi:10.1109/TGRS.2009.2038274

Chaabouni-Chouayakha, H., Rodes Arnau, I., and Reinartz, P., 2013. Towards automatic 3-D change detection through multi-spectral and digital elevation model information fusion. *International Journal of Image and Data Fusion*, 4 (1), 89–101. doi:10.1080/19479832.2012.739577

Comaniciu, D. and Meer, P., 2002. Mean-shift: a robust approach toward feature space analysis. *IEEE Transactions on Pattern Analysis and Machine Intelligence*, 24 (5), 603–619. doi:10.1109/34.1000236

Coppin, P., *et al.*, 2004. Review article: digital change detection methods in ecosystem monitoring: a review. *International Journal of Remote Sensing*, 25 (9), 1565–1596. doi:10.1080/0143116031000101675

Corbane, C., *et al.*, 2011. A comprehensive analysis of building damage in the 12 January 2010 MW7 Haiti earthquake using high-resolution satellite and aerial imagery. *Photogrammetric Engineering & Remote Sensing*, 77 (10), 997–1009. doi:10.14358/PERS.77.10.0997

d'Angelo, P., *et al.*, 2008. Towards automated DEM generation from high resolution stereo satellite images. *International Society for Photogrammetry and Remote Sensing*, 37 (Part B4), 1137–1342.

d'Angelo, P. and Reinartz, P., 2011. Semiglobal matching results on the ISPRS stereo matching benchmark. *In*: *High-resolution earth imaging for geospatial information*, 14–17 June, Hannover.

Dell'Acqua, F., Polli, D.A., and Lisini, G., 2010. Automatic mapping of earthquake damage using post-event radar satellite data: the story goes on. *In*: *30th EARSeL symposium: remote sensing for science, education and culture*, 31 May–3 June, Paris.

Gamba, P. and Casciati, F., 1998. GIS and image understanding for near-real-time earthquake damage assessment. *Photogrammetric Engineering and Remote Sensing*, 64 (10), 987–994.

Haralick, R.M., Shanmugam, K., and Dinstein, I., 1973. Textural features for image classification. *IEEE Transactions on Systems, Man and Cybernetics*, 3 (6), 610–621. doi:10.1109/TSMC.1973.4309314

Hirschmüller, H., 2008. Stereo processing by semiglobal matching and mutual information. *IEEE Transactions Pattern Analysis and Machine Intelligence*, 30 (2), 328–341. doi:10.1109/TPAMI.2007.1166

Hussain, E., *et al*., 2011. Building extraction and rubble mapping for City Port-au-Prince Post-2010 earthquake with GeoEye-1 imagery and LiDAR data. *Photogrammetric Engineering and Remote Sensing*, 77, 1011–1023. doi:10.14358/PERS.77.10.1011

Knudsen, T. and Olsen, B., 2003. Automated change detection for updates of digital map databases. *Photogrammetric Engineering & Remote Sensing*, 69 (11), 1289–1296. doi:10.14358/PERS.69.11.1289

Matikainen, L., *et al*., 2010. Automatic detection of buildings and changes in buildings for updating of maps. *Remote Sensing*, 2, 1217–1248. doi:10.3390/rs2051217

Murakami, H., *et al*., 1999. Change detection of buildings using an airborne laser scanner. *ISPRS Journal of Photogrammetry & Remote Sensing*, 54, 148–152. doi:10.1016/S0924-2716(99)00006-4

Nielsen, A.A., 2007. The regularized iteratively reweighted multivariate alteration detection method for change detection in multi- and hyperspectral data. *IEEE Transactions Image Processing*, 16 (2), 463–478. doi:10.1109/TIP.2006.888195

OpenTopography, 2011. World bank – ImageCat Inc. – RIT haiti earthquake LiDAR dataset. Available from: http://opentopo.sdsc.edu [Accessed 12 May 2011].

Poli, D. and Soille, P., 2012. Digital surface model extraction and refinement through image segmentation application to the ISPRS benchmark stereo dataset. *Photogrammetrie-Fernerkundung-Geoinformation*, 4, 317–329. doi:10.1127/1432-8364/2012/0120

Rastiveis, H., Samadzadegan, F., and Reinartz, P., 2013. A fuzzy decision making system for building damage map creation using high resolution satellite imagery. *Natural Hazards and Earth System Science*, 13 (2), 455–472. doi:10.5194/nhess-13-455-2013

Singh, A., 1989. Review article: digital change detection techniques using remotely-sensed data. *International Journal of Remote Sensing*, 10 (6), 989–1003. doi:10.1080/01431168908903939

Tian, J., 2013. *3D change detection from high and very high resolution satellite stereo imagery*. Dissertation. University of Osnabrück, 1–145.

Tian, J., Cui, S., and Reinartz, P., 2014a. Building change detection based on satellite stereo imagery and digital surface models. *IEEE Transactions on Geoscience and Remote Sensing*, 52 (1), 406–417. doi:10.1109/TGRS.2013.2240692

Tian, J., *et al*., 2011. Region based forest change detection from Cartosat-1 stereo imagery. *International Archives of the Photogrammetry, Remote Sensing and Spatial Information Sciences*, XXXVIII-4/W19, 325–330.

Tian, J., Nielsen, A.A., and Reinartz, P., 2014b. Improving change detection in forest areas based on stereo panchromatic imagery using kernel MNF. *IEEE Transactions on Geoscience and Remote Sensing*, 52 (11), 7130–7139. doi:10.1109/TGRS.2014.2308012

Tian, J., *et al*., 2013. Region-based automatic building and forest change detection on Cartosat-1 stereo imagery. *ISPRS Journal of Photogrammetry and Remote Sensing*, 79, 226–239. doi:10.1016/j.isprsjprs.2013.02.017

Tong, X., *et al*., 2012. Building-damage detection using pre- and post-seismic high-resolution satellite stereo imagery: a case study of the May 2008 Wenchuan earthquake. *ISPRS Journal of Photogrammetry and Remote Sensing*, 68, 13–27. doi:10.1016/j.isprsjprs.2011.12.004

Turker, M. and Cetinkaya, B., 2005. Automatic detection of earthquake-damaged buildings using DEMs created from pre- and post-earthquake stereo aerial photographs. *International Journal of Remote Sensing*, 26 (4), 823–832. doi:10.1080/01431160512331316810

Turker, M. and San, B.T., 2003. SPOT HRV data analysis for detecting earthquake-induced changes in Izmit, Turkey. *International Journal of Remote Sensing*, 24, 2439–2450. doi:10.1080/0143116031000070427

Voigt, S., *et al.*, 2011. Rapid damage assessment and situation mapping: learning from the 2010 Haiti earthquake. *Photogrammetric Engineering and Remote Sensing*, 77 (9), 923–931. doi:10.14358/PERS.77.9.923